Optical near-field interference in the excitation of a bowtie nanoantenna

P. Melchior,[1] D. Bayer,[1] C. Schneider,[1] A. Fischer,[1] M. Rohmer,[1] W. Pfeiffer,[2] and M. Aeschlimann[1]

[1]*Fachbereich Physik and Research Center OPTIMAS, Technische Universität Kaiserslautern, Erwin-Schrödinger-Strasse 46, D-67663 Kaiserslautern, Germany*

[2]*Fakultät für Physik, Universität Bielefeld, Universitätsstrasse 25, D-33516 Bielefeld, Germany*

(Received 14 December 2010; published 8 June 2011)

We show experimentally as well as in simulation that the phase-sensitive superposition of different plasmonic modes leads to a spatially controllable enhancement of the near-field inside and in the vicinity of a metallic nanostructure. Multiphoton photoemission electron microscopy maps the local near-field distribution. By controlling the relative phase Θ between two orthogonally polarized light pulses the spatial distribution of the near-field is manipulated on the basis of the interference of the near-field modes. This demonstration of optical near-field control is corroborated by finite integral time domain calculations.

DOI: 10.1103/PhysRevB.83.235407 PACS number(s): 42.65.Re, 78.47.J−, 79.60.−i, 78.67.−n

I. INTRODUCTION

Optical near-field control in the vicinity of nano-optical antennas is in the focus of the rapidly evolving field of "ultrafast nano-optics" and plays a key role in the research field of plasmonics.[1–7] Merging the fields of nano-optics and ultrafast laser technology has recently opened up a wide range of perspectives in controlling the near fields on a subwavelength length and an ultrafast time scale.[1,8] Coherent control of the near field in the vicinity of nanostructures has been theoretically predicted by the use of broadband chirped laser pulses.[2] In the present context, the coherent control of optical near fields relies on interference phenomena, i.e., the actual near-field distribution and the local excitation depend on the spectral phase of the incoming light. Ultrafast adaptive optical near-field control schemes and the main control mechanism have been investigated in detail, and two main mechanisms for controlling the near-field in the vicinity of nanostructures have been identified in theoretical investigations.[6,7,9] The first is a local interference of optical near-field modes that are excited by two orthogonal polarization components of the incident light. Constructive or destructive interference of these modes is used to control the nanoscale spatial momentary field distribution. The control parameter is the phase difference between the two orthogonal polarization components of the incident far field, i.e., the momentary polarization state of the incident light. The second control mechanism is related to a manipulation of the temporal evolution of the local near field via the spectral phase of linearly polarized incident light. Applying a spectral phase opposite to the phase of the local response function at a given location in the nanostructure leads to a local field evolution with the shortest possible pulse duration, i.e., the chirp of the incident pulse compensates the spectral phase of the local response. This mechanism should allow achieving the highest possible local field strength and thus provides an important control tool to optimize and localize the nonlinear response in a given nanostructure.[7]

The control of optical near fields has been reported using many-parameter adaptive polarization pulse shaping.[3,4] By this technique it became possible to manipulate the optical near-field distribution spatially and temporally on a nanometer spatial scale and a femtosecond time scale.[3,5,7,9,10] In an analytical approach it has been shown that an optimal switching of the near-field intensity between two local areas is achieved if the difference of the spectral phases of the two incident laser pulse polarization components is changed by π.[6] This open-loop optimal control scheme opens new ways to more flexible and more general coherent control in nanophotonics. Both the ultrafast optical nanoscale switching and the optimal control rule rely on the above-mentioned optical near-field interference mechanism. Although this mechanism has been clearly demonstrated in theoretical investigations,[3,6,7] an unambiguous experimental demonstration is still missing. Here we provide a simple but very effective demonstration of these near-field interferences by means of near-field switching in a bowtie-shaped antenna configuration. We use a bowtie nanoantenna as a simple model system since the properties of bowtie-shaped metallic nanostructures as a commonly used nanostructure in the sense of a nano-optical antenna have been investigated theoretically and experimentally.[11,12]

The outline of this work is as follows: In Sec. II we give an overview over the near-field interference mechanism that leads to the controllability of the field distribution. We describe our experimental approach to use a photoemission electron microscope (PEEM) to map the near-field distribution of a nanostructured surface and the combination with ultrafast laser pulse excitation in Sec. III. Additionally, the characteristics of the nanostructures are analyzed, and the simulation characteristics are given. The interfering near-field modes are mapped independently by applying linearly polarized laser pulses with crossed polarizations. In Sec. IV, we present the experimentally achieved near-field distributions and give a comparison with simulated field distributions. Based on this we demonstrate near-field switching as the result of interference of the excited modes in the vicinity of the nanostructure when controlling the relative phase of two perpendicular polarized laser pulses. Simulations support the identification of the control mechanism.

II. INFLUENCE OF THE NANOSTRUCTURE ON THE NEAR-FIELD DISTRIBUTION

The interaction of a nanostructure with an arbitrarily polarized electromagnetic wave can be described as the linear superposition of the responses with respect to two independent polarization components of the incident wave (e.g., TM

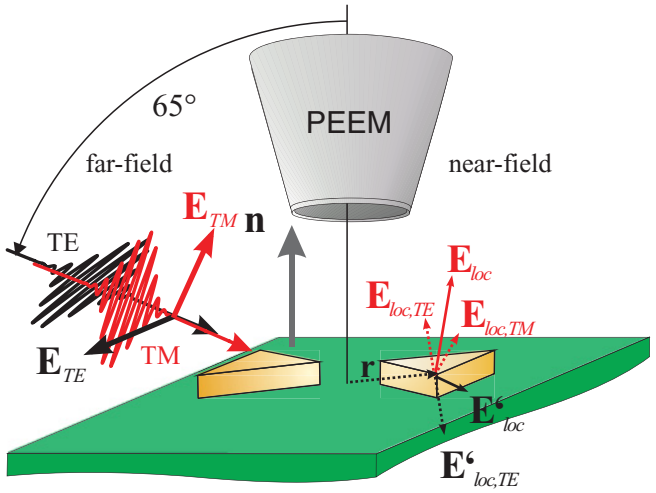

FIG. 1. (Color online) Schematic of the experimental setup and the near-field interference mechanism. The local fields $\mathbf{E}_{\mathrm{loc,TE}}$ and $\mathbf{E}_{\mathrm{loc,TM}}$ generated by the TE and TM far-field components are no longer orthogonal.

and TE) because of the linearity of Maxwell's theory.[3] The propagating far-field components drive the linear polarization $\mathbf{P}_i(\mathbf{r},\omega) = \mathbf{G}_i(\mathbf{r},\omega)\mathbf{E}_{\mathrm{ext},i}(\mathbf{r},\omega)$, which can be described by the space- and frequency-dependent linear local response $\mathbf{G}_i(\mathbf{r},\omega)$, with i = TM, TE. The effective near-field results from the superposition of the induced polarization with the incoming light field $\mathbf{E}_{\mathrm{loc},i}(\mathbf{r},\omega) = [1 + \mathbf{G}_i(\mathbf{r},\omega)]\,\mathbf{E}_{\mathrm{ext},i}(\omega)$. Note that the field components are complex valued and thus contain spectral amplitude and phase for each polarization component. The phase between the two polarization components $\mathbf{E}_{\mathrm{ext,TM}}(\omega)$ and $\mathbf{E}_{\mathrm{ext,TE}}(\omega)$ does not affect the far-field intensity distribution since both components are orthogonal and thus do not interfere. The local fields generated by the two polarization components are, in general, no longer perpendicular to each other, and thus, interference effects between both fields influence the optical near-field distribution in the vicinity of the nanostructures. The local near-field intensity distribution $I_{\mathrm{loc}}(\mathbf{r},\omega)$ includes an interference term that gives the freedom to control the near-field distribution via the phase difference of the two fundamental polarization components. Omitting for simplicity the role of the local magnetic field, the proportionality of the local intensity to the local field components is given by[6]

$$I_{\mathrm{loc}}(\mathbf{r},\omega) \propto |\mathbf{E}_{\mathrm{loc,TM}}(\mathbf{r},\omega)|^2 + |\mathbf{E}_{\mathrm{loc,TE}}(\mathbf{r},\omega)|^2 + 2\,\mathbf{E}_{\mathrm{loc,TE}}(\mathbf{r},\omega)\cdot\mathbf{E}_{\mathrm{loc,TM}}(\mathbf{r},\omega). \quad (1)$$

Figure 1 sketches the corresponding near-field control mechanism. The local optical near-field $\mathbf{E}_{\mathrm{loc}}(\mathbf{r},\omega)$ at the position $\mathbf{r}$ is given by the superposition of the incident light field and the induced polarization fields. Treating both TM and TE components separately, the local field $\mathbf{E}_{\mathrm{loc}}(\mathbf{r},\omega)$ is determined by the relative phase difference $\Theta = \varphi_{\mathrm{TE}} - \varphi_{\mathrm{TM}}$ between them. This means that the polarization state of the incident light determines the local field. The local field component $E^{\alpha}_{\mathrm{loc},i}(\mathbf{r},\omega)$, with $\alpha \in \{x,y,z\}$, for a given linearly polarized incident light at one location $\mathbf{r}$ for one frequency ω is given as a complex number,

$$E^{\alpha}_{\mathrm{loc},i}(\mathbf{r},\omega) \propto \left|E^{\alpha}_{\mathrm{loc},i}(\mathbf{r},\omega)\right| \exp\left[i\,\varphi_i(\mathbf{r},\omega)\right], \quad (2)$$

where i denotes the excitation polarization TM or TE. The superposition of the local fields to calculate the resulting intensity distribution when two independent polarizations are used for excitation can then be expressed using the relative phase Θ. The local electric field components are then given by

$$E^{\alpha}_{\mathrm{loc}}(\mathbf{r},\omega) = \left|E^{\alpha}_{\mathrm{loc,TM}}(\mathbf{r},\omega)\right| \exp[i\,\varphi_{\mathrm{TM}}(\mathbf{r},\omega)] + \left|E^{\alpha}_{\mathrm{loc,TE}}(\mathbf{r},\omega)\right| \exp[i\,\varphi_{\mathrm{TE}}(\mathbf{r},\omega)]\exp(i\,\Theta). \quad (3)$$

A variation of the relative phase Θ by $\Delta\Theta$ corresponds to a phase retardation of one of the fields relative to the other one and is realized in the experiment by a change of the optical delay between two orthogonal polarized laser pulses. Note that the introduced phase difference is not constant over the laser spectrum but shows a linear spectral dependence because of the different involved frequencies. However, in the present case, this influence can be neglected in first-order approximation. Constructive versus destructive interference of the local fields as the phase between the incoming fields is changed gives a handle to control the spatial optical near-field distribution.[5,10] Theoretically, the full information about the response function of a nanostructure is already present if the response of the nanostructure to two orthogonal polarization states of the exciting light is known. All kinds of polarization-dependent effects of the structure can then easily be calculated according to Eq. (3) or generated with the coherent superposition of the two independent polarization states.[7]

III. METHODS AND NANOSTRUCTURE CHARACTERIZATION

A. Photoemission microscopy as a near-field probe

The investigation of nano-optical antennas with tailored designs requires a noninvasive and versatile technique to map the near-field distribution with a sufficiently high spatial resolution and the possibility to resolve the temporal evolution of the optical near-field distribution and nanophotonic excitations. It has been shown that PEEM is a suitable tool to investigate the near fields around nanostructures and their electronic as well as plasmonic properties.[13,14]

Plasmonic resonances of nanostructures made of gold or silver lie in the visible spectral range. Therefore, the photon energy of the corresponding resonance is smaller than the work function Φ of gold used here as nanostructure material. Φ lies, depending on the surface conditions, at about Φ = 4.7–5.1 eV.[15,16] With a photon energy of $h\nu = 1.55$ eV a nonlinear photoemission process is necessary to overcome the work function of the material. In the simplest model for multiphoton photoemission neglecting details of the material band structure, intermediate state lifetimes, and final state effects, the yield is proportional to the $2n$th power of the local electric field $\mathbf{E}_{\mathrm{loc}}(\mathbf{r},\omega)$, where n is the order of nonlinearity. Hence, while the plasmon excitation or, more generally, the optical response of the nanostructure is still in the linear regime, the detected photoemission signal is the result of a nonlinear process.[17] By this the local near-field intensity is enhanced nonlinearly. The higher the order of the process is, the more sensitively the signal reacts to small variations in the near-field intensity.

B. The experimental setup

The experiments are performed with a photoemission electron microscope based on an electrostatic lens system (Focus IS PEEM) with a spatial resolution of <40 nm, situated in an ultrahigh vacuum system. As an excitation source we use a mercury lamp (unpolarized cw light with a cutoff energy of 4.9 eV) or a mode-locked Ti:Sa-laser oscillator that delivers bandwidth-limited laser pulses of 25-fs pulse duration on a center wavelength of $\lambda = 795$ nm with a repetition rate of 80 MHz. The laser beam is focused down to a diameter of about 100 μm on the sample under an angle of incidence of 65°. The sample orientation is sketched in Fig. 1. TM-polarized light contains an in-plane component (parallel to the sample surface) that points along the bowtie antenna axis and a normal component. In contrast, TE-polarized light contains exclusively an in-plane component oriented perpendicular to the antenna axis. Note that the distinction between TM and TE configurations is only related to the incoming light field.

In Sec. IV C we concentrate our discussion on the interference term of the optical near-field modes excited by two orthogonally polarized incident light pulses, i.e., the scalar product in Eq. (1). This term is controlled via the phase between the two pulses using a Mach-Zehnder interferometer. One interferometer path passes a delay stage that enables a variation of the optical path length, while the second part of the beam goes through a periscope that rotates the light polarization from TM to TE polarization. On a second beam splitter the two beams are recombined and propagate collinearly to the experiment. A variation of the delay between the two pulses corresponds to a change of the relative phase between the two field components and by this a variation of the actual polarization state.[7] The stability of the Mach-Zehnder interferometer with respect to vibrations and drift is sufficiently high that phase variations over typical measurement periods of several minutes are negligible. The used delay stage moves the phase in predefined steps of about half the optical wavelength at the center wavelength of the used laser pulses. Note that the absolute phase between both interferometer arms is unknown since a slow unknown phase drift cannot be avoided. Consequently, only the phase difference $\Delta\Theta$ is controlled in the present experiment.

C. Bowtie antenna fabrication and characterization by scanning electron microscopy and one-photon PEEM

The investigated structure is a gold bowtie nanoantenna on an indium tin oxide (ITO) coated glass substrate fabricated with standard electron beam lithography. The single antenna arms consist of triangular-shaped nanoprisms with a thickness of 40 nm and equilateral sides with a length of 350 nm and a gap width of 100 nm. The scanning electron microscopy image [Fig. 2(a)] shows the investigated structure. Small defects and irregularities on the structure edges are caused by the fabrication process. The PEEM image under UV light excitation ($h\nu \leqslant 4.9$ eV) in Fig. 2(b) shows the one-photon photoemission (1PPE) pattern of the bowtie antenna. The emission across the Au surface is rather homogeneous and shows a high contrast to the emission from the ITO substrate. The excitation at 4.9 eV is far detuned from collective resonances of the Au bowtie antennas. The uniform photoemission reflects a homogenous distribution of the internal field. The 1PPE pattern is therefore used to localize the nanoprisms and to visualize the outline of the nanostructure in the recorded multiphoton PEEM patterns (see Fig. 4).

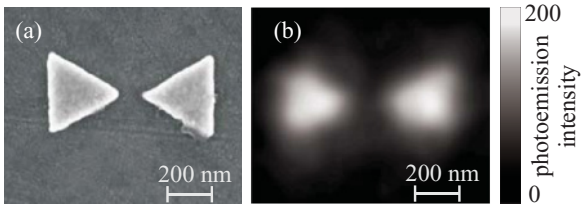

FIG. 2. Comparison of bowtie structure and one-photon photoemission pattern. (a) Scanning electron microscope image of the bowtie nanostructure. (b) One-photon photoemission (1PPE) pattern for UV excitation (unpolarized cw excitation with a cutoff energy of 4.9 eV).

D. Field simulation method

The simulations are performed with the commercial software package CST MICROWAVE STUDIO based on the finite integral method (FIM).[18,19] The parameters used correspond to those of the experimental structure, i.e., a prism side length of 350 nm and a gap between the triangular prisms of 100 nm. The corners and edges of the nanoprisms are rounded with a radius of curvature of 10 nm. We used a plane-wave excitation with an angle of incidence of 65° to the surface normal in accordance with the experimental conditions. The discretization mesh step has been chosen to be 0.85 nm in the direct vicinity of the structure; in the outer simulation volume, a bigger mesh size up to 17 nm has been applied in order to reduce the calculation time. The discretization size is sufficiently small for a convergence and high accuracy of the algorithm. This has been checked with an adaptive mesh optimization that logs the total cross section with every simulation run. The optimum mesh-size configuration has been reached when a predefined convergence criterion has been met. The criterion here uses the deviation of the total scattering cross section between two sequential mesh-refinement runs of less than 1%. The excitation spectrum has been set to cover the spectral range from $\nu = 300$ to 450 THz (corresponding to $\lambda = 1000$–660 nm) with a Gaussian envelope, centered at 375 THz and 80 THz full width half maximum (FWHM). For the calculation the dielectric properties of the structure material (gold) are taken from the experimental data from Landolt-Boernstein[20] and have been fitted with a polynomial expression of the order of 6. The maximal deviation of the fitted curve lies in the range of less than 2.5%. The nanostructure has been modeled to sit on an ITO substrate. Also, the material properties of ITO have been taken into account as for the metal structure.[21] The substrate has been chosen large enough to reduce artifacts from reflections caused by an insufficient efficiency of the perfectly matched layer at the boundaries.

The response of the structure to an illumination with the broadband wave has been logged at certain points of interest. Figure 3 shows the response at a single corner of the bowtie structure for TM and TE excitation about 0.5 nm below the metal surface inside the material. We show the response

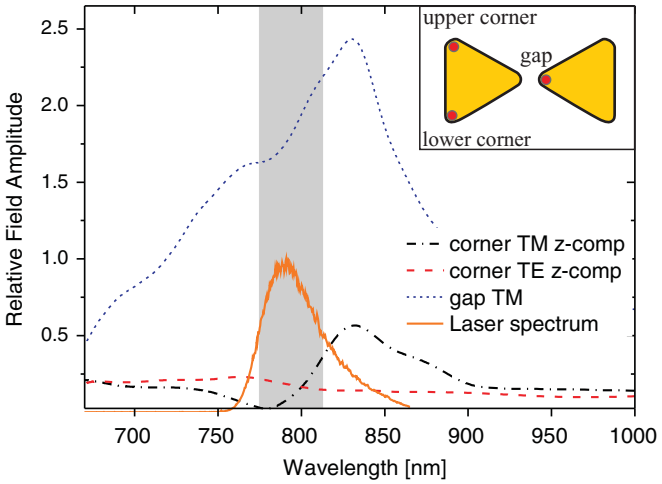

FIG. 3. (Color online) Simulated near-field response (z component) recorded at a single corner of the left nanoprism for TE (red dashed line) and TM (black dash dotted line) polarized excitation of a bowtie nanoantenna. The blue dotted line shows the response at the gap corner of the right nanoprism. The shadowed area shows the bandwidth (FWHM) of the laser pulses used with a maximum at $\lambda = 795$ nm (yellow solid line). The inset sketches the points of interest.

inside the metal as only the internal field is relevant for the photoexcitation into intermediate bound states and thus also dominates the multiphoton photoemission process. We focus our investigation in this work on the near-field interference and show therefore in Fig. 3 the local response only at the outer corner of the bowtie structure where we present the interference effect later on.

The local field components $E^{\alpha}_{\mathrm{loc},i}(\mathbf{r},\omega)$, with $\alpha \in \{x,y,z\}$, as derived from the FIM calculations for TM- and TE-polarized illumination are composed like in Eq. (3) to simulate a simultaneous excitation with TM and TE polarization. The influence of the interference term [the term on the right-hand side of Eq. (1)] is investigated by a variation of the phase difference between the two independent excitation fields, as will be discussed in detail in Sec. IV C.

IV. RESULTS AND DISCUSSION

A. Near-field modes: Experiments

Applying a femtosecond laser pulse to the nanostructure as shown in Fig. 2 with a photon energy of $h\nu = 1.55$ eV, a hot-spot-like photoemission pattern is observed [see Figs. 4(b) and 4(c)]. The emission pattern no longer follows the shape of the nanoantenna but is now localized in distinct regions of the structure depending on the polarization state of the incident light. Note that the comparison with 1PPE images [see Fig. 4(a)] obtained under UV excitation and the identical settings of the PEEM apparatus allows determining the exact position of the hot-spot photoemission on the structure (outlines in Fig. 4).

For TM-polarized excitation an emission maximum in the gap region is clearly resolved [Fig. 4(b)]. The unambiguously located nanostructure outline in this emission pattern shows that the emission maximum is centered at the tip of the right nanoprism rather than in the middle of the gap. In

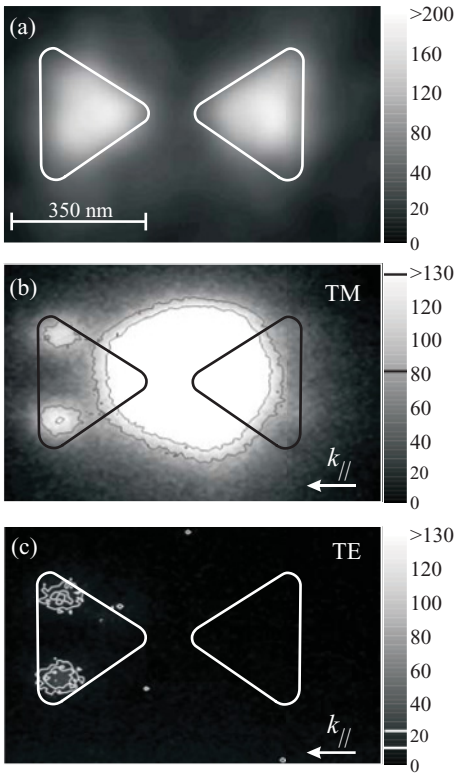

FIG. 4. Photoemission pattern from the bowtie antenna. (a) 1PPE pattern (off-resonant) obtained under UV excitation using a mercury lamp. (b) 3PPE pattern under TM-polarized laser pulse excitation reveals strong photoemission from the antenna gap and a weak photoemission at the corners of the left nanoprism. (c) 3PPE pattern under TE-polarized laser pulse excitation shows weak photoemission from the corners of the left nanoprism. The laser beam comes from the right side and is indicated by the parallel k vector component $k_{\parallel}$.

addition to this strong "gap emission" in Fig. 4(b), smaller emission maxima appear at the outer corners of the triangular nanoprisms. Interestingly, these weak photoemission maxima appear at the left nanoprism only. This asymmetry is attributed to the non-normal illumination condition, i.e., the parallel component $k_{\parallel}$ of the incident light is directed toward the left. Due to the non-normal incidence of the light and the size of the structure, which is in the order of one wavelength of the light, the response of the nanostructure is influenced by the retardation effect.

Under TE excitation [Fig. 4(c)] the emission pattern of the nanoantenna changes significantly. The gap area of the bowtie structure exhibits no emission. Only the upper and lower corners of the left triangular nanoprism appear to be weakly pronounced. The yield at the corners of the left nanoprism is under TE excitation with the same laser intensity about ten times weaker than for TM excitation. The intensity dependence of the total photoemission yield indicates that at least a three-photon process is responsible for the detected emission, i.e., the yield scales with the sixth power of the electric field. Therefore, the electric fields at the corners of the left nanoprisms are still of the same magnitude, although we observe a strong difference in the photoemission signal.

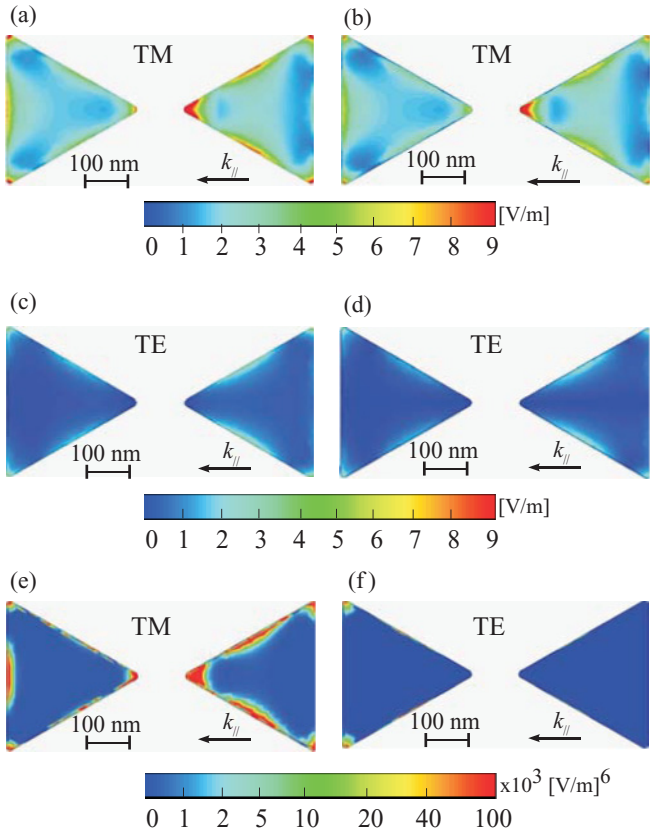

FIG. 5. (Color) Simulated field distribution on the surface of the gold nanostructure at a wavelength of $\lambda = 795$ nm. The illumination geometry is as in Fig. 1, with the light coming from the right side as indicated by the arrow denoted with $k_{||}$. (a) Relative amplitude of the local electric field and (b) its z component for TM-polarized illumination. (c) and (d) Relative amplitude and z component for TE-polarized illumination. (e) and (f) Sixth power of the simulated field (E_z component) in logarithmic scale to qualitatively compare the distribution with PEEM images from a 3PPE process. The incident field has an amplitude of 1 V/m.

For the following discussion it should be emphasized that there is no obvious difference in the photoemission yield between the upper and the lower outer corners of the left nanoprism. For purely linear polarized TM or TE light this behavior is fully expected because of the symmetry of the nanostructure. As will be shown later in this work (see Sec. IV C), this changes dramatically when the excitation field simultaneously contains TM and TE components.

B. Near-field modes: Simulations

Figure 5 shows the calculated field amplitude on the surface of the gold nanostructure for the wavelength of $\lambda = 795$ nm. The excitation light comes from the right side under an angle of 65° to the surface normal, where $k_{||}$ indicates the vector component parallel to the surface. Figures 5(a) and 5(c) present the absolute value of the field for TM and TE excitations. The field is dominated by the z component of the electric field on the surface of the metallic structure proven in Figs. 5(b) and 5(d). The contour plots in Figs. 5(a)–5(d) are shown on the same linear scale. The direct comparison reflects that the overall induced field amplitude under TE-polarized excitation is much weaker in the gap area of the bowtie structure and slightly weaker in the area around the edges as compared to TM excitation. For TM excitation [see Figs. 5(a) and 5(b)] a strong field enhancement occurs in the gap area of the bowtie antenna and at the corners of the prisms. As can be seen from Fig. 3, the gap mode resonance has its maximum at a wavelength of 825 nm. The center wavelength of the laser pulse is therefore blue shifted to the structure resonance. The slightly off-resonant excitation of this mode leads only to a moderate field enhancement, and thus, the effects of the corner and edge modes can still be resolved in the multiphoton photoemission pattern. Figures 5(c) and 5(d) show the spatial distribution for the total electric field strength and its z component in the case of TE-polarized excitation. In contrast to a TM-polarized excitation, the structure does not show a clear resonance peak in the response function for TE polarization but is rather flat in the interesting wavelength range (compare Fig. 3).

To qualitatively compare the calculation with the PEEM results, it is necessary to consider the nonlinearity of the 3PPE process. Figures 5(e) and 5(f) show therefore the sixth power of the calculated electric field (E_z component) and thus should correspond qualitatively to the emission pattern generated in a three-photon photoemission process. The spatial field distributions in Fig. 5(e) and 5(f) are plotted on logarithmic scale as they cover a huge dynamic range.

The calculated distributions show good agreements with the PEEM patterns (compare Fig. 4). Figure 5(e) shows the simulated nonlinear emission pattern for a TM-polarized excitation. The strong field in the gap area of the bowtie structure is about one order of magnitude larger than at the outer corners of the right nanoprism. The experimental PEEM pattern [see Fig. 4(b)] shows, in good agreement with that for TM polarization, a strong peak signal in the gap area located at the tip of the right nanoprism that is about a factor of 30 higher than the two weak signal peaks at the outer corners of the left nanoprism. In contrast to the simulated distributions, we do not see a photoemission from the basis edge on the left side and from the edges of the right prism.

The calculated distribution for TE-polarized excitation [see Fig. 5(f)] is also in good agreement with the experimental data in Fig. 4(c). The measured photoemission signal is very small except for the outer corners of the left nanoprism. This is also seen in the calculated distribution, i.e., only the outer corners of the left prism show a pronounced field.

C. Optical near-field mode interferences in bowtie nanoantennas

In the following we show experimentally as well as in simulation that the superposition of the near fields leads to a phase-sensitive intensity distribution that is determined by the interference term in the intensity profile. A Mach-Zehnder interferometer is used to coherently superpose two laser pulses with cross-polarized electric fields as described above. Changing the optical path length of one of the beams on a nanometer scale corresponds to a relative phase shift between both pulses and thus also between the two polarization components. So the actual polarization state of the incident light can be controlled. The center wavelength of both laser beams is $\lambda = 795$ nm,

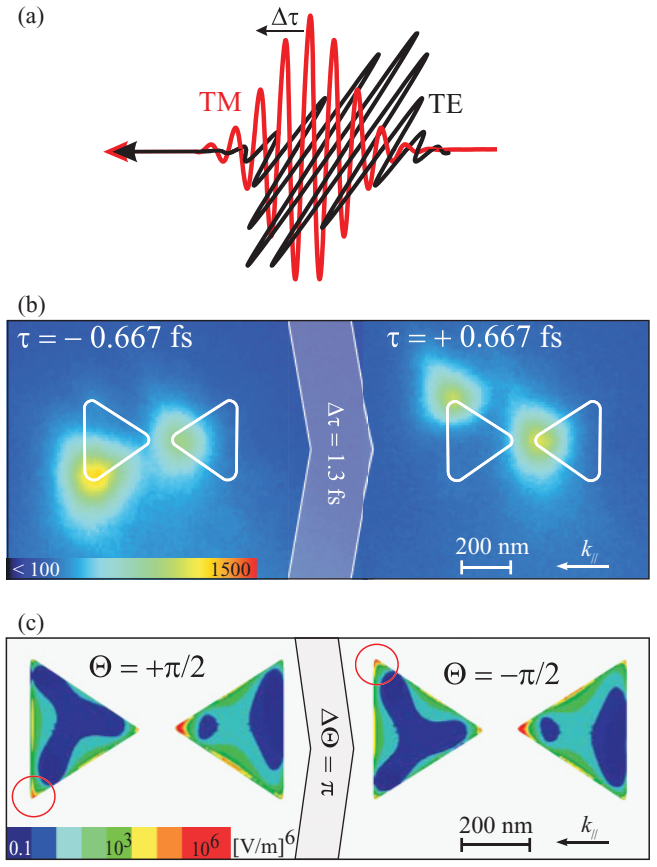

FIG. 6. (Color) (a) Control scheme for manipulation of the near-field distribution with two cross-polarized laser pulses. (b) Switching of the photoemission maxima at the outer corners of the left nanoprism. (c) Simulated 3PPE pattern in logarithmic scale. The images show the resulting intensity distribution after a linear superposition of the calculated field distributions for TM- and TE-polarized excitation with a relative phase of $+\pi/2$ and $-\pi/2$, respectively, i.e., left and right circular polarized light.

and the corresponding oscillation period of the electric field is 2.66 fs. The delay control between the two laser pulses with the delay stage used is achieved via discrete delay steps $\Delta\tau$ of about 0.66 fs. A two-step variation of the path length changes the phase between the TM- and TE-polarized laser pulses correspondingly by about $\Delta\Theta = \pi$. Note that the absolute phase between both interferometer arms is unknown in the present experiment.

Figure 6(b) shows the experimental results of the interferometric superposition of TM- and TE-polarized lasers. The two PEEM images represent two different time delays between the two laser pulses. The photoemission signal from the tip at the antenna gap does not change significantly when the time delay between the pulses is changed. In contrast, the photoemission signal changes from the lower to the upper corner of the left nanoprism when the delay is changed by 1.33 fs. This corresponds to an additional phase of $\Delta\Theta = \pi$ between the two polarization components [compare Eq. (3)]. The photoemission signal is related to the local field strength. Thus, the switching in the photoemission pattern reveals that the local excitation depends on the relative phase of the two polarization components. We therefore attribute the local emission switching to either constructive or destructive interference of the local fields excited by the two orthogonal far-field polarization components. An efficient change in the local intensity can only be reached if the interference term in Eq. (1) has a magnitude similar to the local intensities generated by the two components independently. This is only the case if the superimposed fields are of the same order of magnitude. As can be seen from Figs. 4 and 5, this is only fulfilled at the outer corners of the left nanoprism. In the gap area, there is no significant field for TE polarization, and so no interference between the TE and TM mode occurs. The PEEM experiments [Fig. 6(b)] and the numerical simulation [Fig. 6(c)] agree perfectly if one considers that the calculated distribution must be convoluted with a spatial resolution of the PEEM of about 40 nm.

The calculated field distributions shown in Fig. 6 combined with the complex phase of the field already contain all the information necessary to reproduce the phase-sensitive behavior of the photoemission pattern when changing the relative phase between TM and TE excitation. According to Eqs. (2) and (3), we used the complex form of the electric field to calculate the near-field distribution for a combined excitation with TM and TE polarization. A variation $\Delta\Theta$ of Θ changes the polarization state of the incident light and therefore also affects the nanostructure excitation. Figure 6(c) shows the third power of the intensity of the z component of the local field after superposing the calculated field distributions for TM- and TE-polarized excitation with relative phase differences of $\Theta = +\pi/2$ and $\Theta = -\pi/2$. One can see that the high yield at the outer corners of the left nanoprism moves from the lower to the upper side as the phase relation is changed by an additional phase difference of $\Delta\Theta = \pi$. We interpret this as the result of the interference of two local fields at the edges of the prisms that are generated by two orthogonal polarization components. Note that this is a proof of principle experiment done on a geometrical simple nanostructure. A relative phase difference $\Delta\Theta = \pi$ between the two independent light polarizations results for an initial $\Theta = -\pi/2$ in switching from left to right circular polarization. Indeed, a test experiment by means of an excitation with circular polarized light generated with a quarter wave plate results in the same local near-field distributions.

V. CONCLUSION AND OUTLOOK

In a proof of principle experiment we experimentally demonstrate the impact of optical near-field interference on the local excitation in a nanostructure, i.e., a gold bowtie nanoantenna. Simple phase-sensitive interferometric superposition of two laser pulses with crossed polarizations (TM and TE modes) allows the switching of the local excitation between the upper and lower corners of one particular nanoprism of the antenna structure. Each polarization induces a symmetric photoemission behavior. If the structure is illuminated simultaneously with TM- and TE-polarized laser pulses, the coherent interaction of the different local modes leads to an effective field distribution that strongly depends on the relative phase Θ. This dependency can be visualized in terms of switching the photoemission localization by changing

the relative phase between the two laser pulses. The scalar product of the induced local fields for TM and TE excitation has a magnitude similar to the local field intensities of TE- and TM-induced fields independently and thus gives rise to a high contrast between constructive and destructive interference of local fields. Numerical field calculations support our interpretation of the intensity switching as a near-field interference effect based on the phase-sensitive superposition of independent near-field modes. Note that this effect is not limited to this specific nanostructure geometry of a bowtie antenna to observe near-field interferences. The only requirement is the existence of different modes that can be addressed by independent far-field components of the electric field and that result in a similar local electric field strength.

The presented experiment demonstrates a simple implementation of a control scheme for the optical near-field distribution of a plasmonic nanostructure. This technique is an easy approach to gain insight in the interaction of local excitations in order to optimize the nanostructure design and analyze their near-field properties.

ACKNOWLEDGMENTS

We thank the DFG for support within the Research Focus Program "Ultrafast Nano-Optics" (SPP 1391) and the NBC (Nano- and Bio-Center) of the University of Kaiserslautern for sample preparation. This work was also supported by the post graduate program GRK 792 of the DFG (to C.S. and P.M.).

[1] P. Vasa, C. Ropers, R. Pomraenke, and C. Lienau, Laser Photonics Rev. **3**, 483 (2009).
[2] M. I. Stockman, S. V. Faleev, and D. J. Bergman, Phys. Rev. Lett. **88**, 067402 (2002).
[3] T. Brixner, F. J. García de Abajo, J. Schneider, and W. Pfeiffer, Phys. Rev. Lett. **95**, 093901 (2005).
[4] M. Sukharev and T. Seideman, Nano Lett. **6**, 715 (2006).
[5] M. Aeschlimann, M. Bauer, D. Bayer, T. Brixner, F. J. García de Abajo, W. Pfeiffer, M. Rohmer, C. Spindler, and F. Steeb, Nature (London) **446**, 301 (2007).
[6] P. Tuchscherer, C. Rewitz, D.V. Voronine, F. J. Garcia de Abajo, W. Pfeiffer, and T. Brixner, Opt. Express **17**, 14235 (2009).
[7] J. S. Huang, D. V. Voronine, P. Tuchscherer, T. Brixner, and B. Hecht, Phys. Rev. B **79**, 195441 (2009).
[8] M. I. Stockman, New J. Phys. **10**, 025031 (2008).
[9] T. Brixner, F. J. García de Abajo, J. Schneider, C. Spindler, and W. Pfeiffer, Phys. Rev. B **73**, 125437 (2006).
[10] M. Aeschlimann, M. Bauer, D. Bayer, T. Brixner, S. Cunovic, F. Dimler, A. Fischer, W. Pfeiffer, M. Rohmer, C. Schneider, F. Steeb, C. Strueber, and D.V. Voronine, Proc. Natl. Acad. Sci. USA **107**, 5329 (2010).
[11] D. P. Fromm, A. Sundaramurthy, P. J. Schuck, G. Kino, and W. E. Moerner, Nano Lett. **4**, 957 (2004).
[12] J. Boneberg, J. Konig-Birk, H. J. Munzer, P. Leiderer, L. Shuford, and C. Schatz, Appl. Phys. A **89**, 299 (2007).
[13] M. Cinchetti, A. Gloskovskii, S. A. Nepjiko, G. Schönhense, H. Rochholz, and M. Kreiter, Phys. Rev. Lett. **95**, 047601 (2005).
[14] A. Oelsner, M. Rohmer, C. Schneider, D. Bayer, G. Schönhense, and M. Aeschlimann, J. Electron Spectrosc. **178-179**, 317 (2010).
[15] P. A. Anderson, Phys. Rev. **115**, 553 (1959).
[16] H. B. Michaelson, J. Appl. Phys. **48**, 4729 (1977).
[17] M. Merschdorf, C. Kennerknecht, and W. Pfeiffer, Phys. Rev. B **70**, 193401 (2004).
[18] T. Weiland, Int. J. Numer. Modell. Electron. Devices Fields **9**, 295 (1996).
[19] M. Clemens and T. Weiland, Prog. Electromagn. Res. **32**, 65 (2001).
[20] C. Calandra, *Landolt-Boernstein Numerical Data and Functional Relationships in Science and Technology Physics of Solid Surfaces* (Springer, Heidelberg, 1993).
[21] V. Craciun, C. Chiritescu, F. Kelly, and R. K. Singh, J. Optoelectron. Adv. Mater. **4**, 21 (2002).